Noise-Induced Quenched Disorder in Dense Active Systems

Guozheng Lin,[1] Zhangang Han,[1,*] Amir Shee,[2] and Cristián Huepe[1,2,3,†]
[1]School of Systems Science, Beijing Normal University, Beijing 100875, People's Republic of China
[2]Northwestern Institute on Complex Systems and ESAM, Northwestern University, Evanston, Illinois 60208, USA
[3]CHuepe Labs, 2713 West August Boulevard No. 1, Chicago, Illinois 60622, USA

(Received 20 April 2023; accepted 15 September 2023; published 17 October 2023)

We report and characterize the emergence of a noise-induced state of quenched disorder in a generic model describing a dense sheet of active polar disks. In this state, self-propelled disks become jammed with random orientations, only displaying small fluctuations about their mean positions and headings. The quenched disorder phase appears at intermediate noise levels, between moving polar order and standard dynamic disorder. We show that it results from retrograde forces produced by angular fluctuations with Ornstein-Uhlenbeck dynamics, compute its critical noise, and argue that it could emerge in a variety of systems.

DOI: 10.1103/PhysRevLett.131.168301

Active agents convert stored or ambient energy into mechanical work, injecting it at the smallest scales of the system [1–5]. They typically introduce activity through some form of self-propulsion, interact with neighbors via alignment or attraction-repulsion forces, and can be affected by noise. Many different models of active systems have been studied in recent years, with multiple parameter combinations, which could have potentially resulted in a variety of regimes and nonequilibrium phases. Only a few have been identified up to now, however, corresponding to self-organized states with various forms of (polar or nematic) orientational order [6–8], clustering [9–12], or phase separation [13,14]; as well as to disordered states where agents move in randomly changing directions.

One of the most studied phases displaying orientational order is characterized by collective motion, a state in which all agents are aligned and head in a common direction [15,16]. Examples of collective motion can be found in different types of biological systems, including cytoskeleton-motor proteins [17–19], bacterial colonies [20–22], insect swarms [23,24], bird flocks [25,26], and fish schools [27–30]. It can also develop in artificial systems, such as active colloidal suspensions [11], colloidal rollers [31,32], vibrated polar disks [33,34], or robot swarms [35–42]. This type of self-organization was originally thought to require local alignment interactions [43], but has now been shown to also emerge from a local coupling between attraction-repulsion forces and heading directions [44,45]. Regardless of the underlying mechanism, collective motion corresponds in all these cases to an ordered phase of aligned agents that emerges from a disordered phase. Additionally, both phases are sometimes subdivided into parameter regions with different density distributions [9,10,12,14,46–51].

Beyond collective motion, other collective states have been identified more recently in elastic or jammed active solids [52–56]. Here, attraction-repulsion forces or steric interactions between densely packed agents can result in different forms of collective oscillations and disordered dynamics. Despite some initial studies, very little is still known about the spatiotemporal states that can develop in these cases.

In this Letter, we report the emergence of a noise-induced state of *quenched disorder* (QD) in densely packed active systems, in which agents become jammed with random orientations. The QD phase appears at intermediate noise levels. For lower noise, the systems self-organize into a state of collective motion that we will refer to as moving order (MO); for higher noise, they reach a standard state of dynamic disorder (DD) where all heading are randomly changing. We characterize the QD phase in a generic, minimal model (that represents a natural extension of existing experiments), consisting of a set of densely packed self-propelled disks with off-centered rotation and repulsive interactions. These are similar to the active polar disks and robots with steric interactions introduced in [33,34] and [57], but with linear repulsive forces and anisotropic translational damping, as in [56]. Using this model, we identify the mechanism that leads to QD, describe it analytically, and show that it could develop in a broad range of active systems.

We consider self-propelled polar disks with rotation axes located behind their centroids (geometrical centers), interacting through linear repulsive forces. These can be viewed as a minimal representation of self-propelled agents that are nonaxisymmetric about their centers of rotation, which results in tangential forces that introduce torques. Figure 1(a) illustrates the interaction between two such disks, i and j, with radii $l_0/2$ and self-propulsion heading directions $\hat{n}_i$ and $\hat{n}_j$. Their axes of rotation $\vec{r}_i$ and $\vec{r}_j$ are positioned at a distance $0 \leq R \leq l_0/2$ behind their centroids, so R controls the degree of eccentricity of their rotational

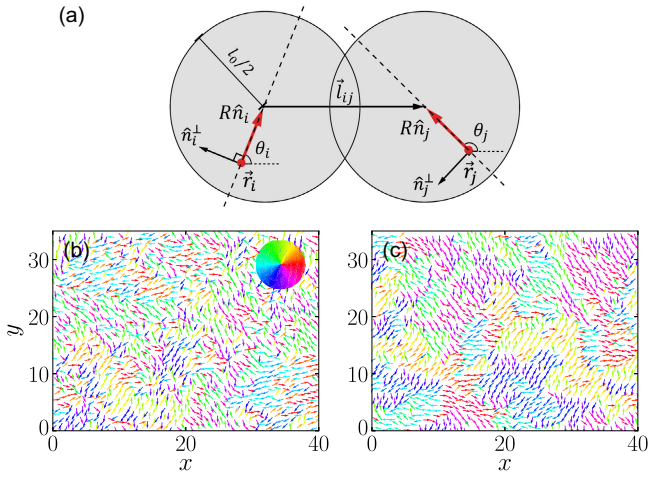

FIG. 1. Top: Schematic representation of the interaction between two self-propelled disks (a) with repulsion radii $l_0/2$ and headings $\hat{n}_i$, $\hat{n}_j$ that can rotate about axes $\vec{r}_i$, $\vec{r}_j$, located a distance R behind each centroid. The repulsion is proportional to $|\vec{l}_{ij}| - l_0$ and projected onto each centroid, resulting in forces and torques about $\vec{r}_i$ and $\vec{r}_j$. Bottom: Snapshots of typical quenched disorder states obtained in a periodic arena, starting from randomly oriented (b) or fully aligned (c) headings. Each disk is represented by an arrow that starts at its centroid, points in its heading direction, and is colored by heading angle as shown in the inset.

motion. This implies that, for small R, the interactions will mainly affect disk positions, whereas for large R, they will mainly affect their headings.

We define the interaction between two disks as a linear repulsive central force, given by $\vec{f}_{ij} = k(|\vec{l}_{ij}| - l_0)\vec{l}_{ij}/|\vec{l}_{ij}|$ if $|\vec{l}_{ij}| \leq l_0$, and by $\vec{f}_{ij} = 0$ otherwise. Here, k determines the repulsion strength and $\vec{l}_{ij}$ is the vector that joins both centroids, which can be expressed in terms of the headings and the axes positions as $\vec{l}_{ij} = (\vec{r}_j - \vec{r}_i) + R(\hat{n}_j - \hat{n}_i)$. The total force over disk i is the sum of pairwise interactions $\vec{F}_i = \sum_j \vec{f}_{ij}$, where $j \in S_i$ is the set of all disks with $|\vec{l}_{ij}| \leq l_0$. Note that, if we added linear attraction forces between neighbors for $|\vec{l}_{ij}| > l_0$, this model would describe the active elastic sheet introduced in [54], formed by an hexagonal array of self-propelled rods with front tips permanently linked by linear springs.

By decomposing the effect of the total interactions $\vec{F}_i$ over the centroid of each disk i into displacement forces and torques about its axis of rotation, we can write the following overdamped dynamical equations [58]

$$\dot{\vec{r}}_i = v_0\hat{n}_i + \hat{n}_i\hat{n}_i^T(\alpha_\parallel\vec{F}_i + \sqrt{2D_\parallel}\vec{\zeta}_i) + (\mathbb{I} - \hat{n}_i\hat{n}_i^T)(\alpha_\perp\vec{F}_i + \sqrt{2D_\perp}\vec{\zeta}_i), \quad (1)$$

$$\dot{\hat{n}}_i = \beta(\mathbb{I} - \hat{n}_i\hat{n}_i^T)\vec{F}_i + \sqrt{2D_\theta}\eta_i(t)\hat{n}_i^\perp. \quad (2)$$

Here, v_0 is the self-propulsion speed and $\hat{n}_i^\perp$ is a unit vector perpendicular to $\hat{n}_i$. Note that, in order to consider a more general model, we included the possibility of having different damping and noise levels for the disk rotation and its front-back and sideways motion, introducing anisotropies in the translational dynamics. Rotation is controlled by the inverse rotational damping coefficient β and the angular diffusion constant D_θ, whereas translation is controlled by the inverse damping coefficients $\alpha_\parallel$, $\alpha_\perp$ and the diffusion constants $D_\parallel$, $D_\perp$ (along $\hat{n}_i$, $\hat{n}_i^\perp$, respectively) [37,54]. Angular noise is added through a delta-correlated Gaussian random variable η_i, with $\langle\eta_i\rangle = 0$ and $\langle\eta_i(t)\eta_j(t')\rangle = \delta_{ij}\delta(t-t')$. Positional noise, through a delta-correlated Gaussian random vector $\vec{\zeta}_i = (\zeta_i^x, \zeta_i^y)$, where $\langle\vec{\zeta}_i\rangle = 0$, $\langle\zeta_i^k(t)\zeta_j^l(t')\rangle = \delta_{ij}\delta_{kl}\delta(t-t')$, and indexes k and l represent x or y.

We carried out simulations of N self-propelled polar disks, using the stochastic Euler method to integrate Eqs. (1) and (2) synchronously for all disks in a periodic rectangular arena of size $l_0\sqrt{N} \times l_0\sqrt{3N}/2$. For N even, this fits exactly $\sqrt{N} \times \sqrt{N}$ disks in a perfect hexagonal lattice with distance l_0 between the centroids of all neighbors. This spatial configuration was used as initial condition, with all angles either aligned in the x direction or selected at random. As we explored the phase space, we found three possible steady states: MO, DD, and QD. States MO and DD have been well documented in the literature, as they correspond to the standard order-disorder (flocking) transition in collective motion. Instead, state QD had not been previously reported and will be the focus of what remains of this Letter.

Figures 1(b) and 1(c) display examples of the QD states obtained in our simulations. Panel (b) is a snapshot of the stationary state reached starting from random initial angles and panel (c) is the corresponding snapshot starting with all headings aligned. The latter presents larger domains of locally aligned agents, showing that the final spatial distribution depends on the initial condition. In both cases, all disks are jammed when the QD state is reached, presenting fixed mean positions and orientations. Note, however, that we sometimes observe localized disk rearrangements, especially in smaller systems, but only at very long timescales.

Our phase space explorations found that QD appears for a significant range of parameter combinations, as shown in the Supplemental Material [58], but not in the often studied case with fully isotropic damping ($\alpha_\parallel = \alpha_\perp$), or in cases with no angular noise ($D_\theta = 0$) or no rotational anisotropy ($R = 0$). In order to study the emergence of QD in the simplest possible context, we will thus focus on a limit case with $\alpha_\perp = D_\parallel = D_\perp = 0$, but where $\alpha_\parallel > 0$ and $D_\theta > 0$. In addition, we will set most parameters in all simulations below, using $v_0 = 0.002$, $\alpha_\parallel = 0.02$, $\beta = 1.2$, $k = 5$, $l_0 = 1$, $N = 1600$, and timestep $dt = 0.01$, while varying D_θ and R.

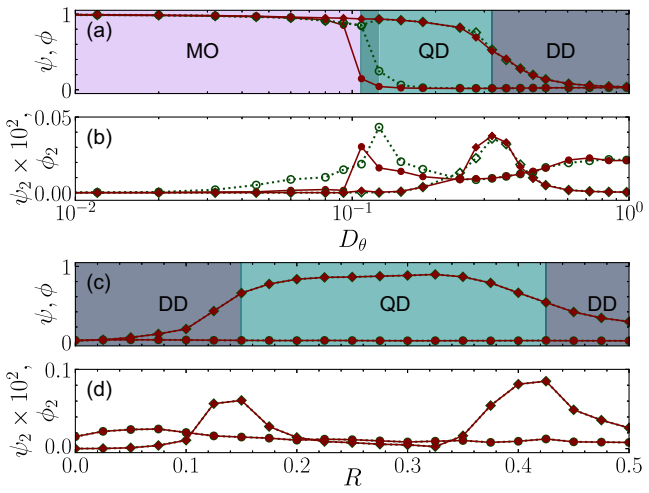

FIG. 2. Order parameters (a),(c) and respective variances (b), (d), as a function of the angular noise D_θ for fixed $R = 0.3$ (a),(b), and of the degree of rotational eccentricity R for fixed $D_\theta = 0.2$ (c),(d). We display the standard polarization ψ (circle) and the orientation persistence ϕ (diamond), using solid or open symbols for randomly oriented or aligned initial conditions, respectively. We identify three regimes: a high ψ, high ϕ moving order (MO) state; a low ψ, high ϕ quenched disorder (QD) state; and a low ψ, low ϕ dynamic disorder (DD) state. Each point is the average of the last 2×10^6 time steps (of 2×10^7 total), after reaching the steady state.

To analyze our results, we introduce 2 order parameters that allow us to discriminate between the collective states. The first one corresponds to the standard polarization $\psi = \langle \| \sum_{i=1}^{N} \hat{n}_i \| \rangle_t / N$ (where $\langle \cdot \rangle_t$ is the average over time after reaching a steady state). It determines the degree of alignment between agents, with $\psi = 1$ if all are perfectly aligned and $\psi = 0$ if they are randomly oriented. The second one evaluates the persistence of the orientation of each agent over time, averaged over all agents, and is defined by $\phi = \sum_{i=1}^{N} \| \langle \hat{n}_i \rangle_t \| / N$. If all orientations are fluctuating about fixed mean values, we have $\phi = 1$; if they are rotating, $\phi = 0$.

Figure 2 presents the three phases obtained in our simulations, as a function of D_θ for fixed $R = 0.3$ (a), (b), and of R for fixed $D_\theta = 0.2$ (c),(d). Panels (a) and (c) show the steady state values of ψ (circles) and ϕ (diamonds), starting from either aligned (open symbols) or random (solid symbols) headings. In panel (a), we find the MO phase at low D_θ, where agents display long-range polar order and persistent orientation ($\psi \approx \phi \approx 1$). At high D_θ, for either low or high R values, we find the DD phase, with continuously changing random headings and positions ($\psi \approx \phi \approx 0$). Finally, at intermediate D_θ and R values, we find the QD phase, where agents are jammed and have orientations that fluctuate about constant random angles ($\psi \approx 0$ and $\phi \approx 1$). Panels (b) and (d) display the respective variances, ψ_2 (circles) and ϕ_2 (diamonds). We define the boundaries between phases as their maxima, finding that the transition between MO and DD occurs at a slightly lower critical D_θ when starting from randomly oriented, rather than aligned, initial conditions.

We now describe the mechanism that leads to the QD state and postulate an approximate representation of its dynamics that will allow us to describe it analytically. We begin by noting that, in a densely packed system and for large enough R, the disks will be blocked from rotating by neighboring agents. This implies that the angular fluctuations generated by noise will be constrained by forces resulting from the repulsive potential between disks. The tangential components of these forces will become restitution forces that oppose angular fluctuations, while most of their radial components will become retrograde forces towards $-\hat{n}_i$. We will show below that the angular dynamics are well described by an Ornstein-Uhlenbeck process [64] and that the transition from the MO phase to the QD phase will occur when these retrograde forces match self-propulsion.

First, we compute the effective angular restitution force that results from the repulsion of neighboring disks. For small angular fluctuations $\Delta\theta(t)$ about the equilibrium orientation $\Delta\theta = 0$, the arc followed by the centroid of each disk can be approximated by a linear displacement $\Delta x = R\Delta\theta$. In the packed case considered here, the agents will thus feel an effective mean restitution force approximately given by $\vec{f} \cdot \hat{n}^{\perp} \approx -(k/c)\Delta x$, where c is a proportionality constant that results from averaging over all configurations of neighbor positions and angular fluctuations. If we then replace this expression into the Eq. (2), we find that, at first order in $\Delta\theta \ll 1$, the disks' mean-field angular dynamics reduce to an Ornstein-Uhlenbeck process [64] described by

$$\dot{\Delta\theta} = -\frac{\beta k R}{c}\Delta\theta + \sqrt{2D_\theta}\eta(t), \tag{3}$$

where $\eta(t)$ is a random variable equivalent to the $\eta_i(t)$ of all disks. The mean-square fluctuations of the orientations over time will thus be equal to [64]

$$\langle \Delta\theta^2 \rangle(t) = \frac{cD_\theta}{\beta k R}(1 - e^{-2\beta k R t/c}). \tag{4}$$

Figure 3(a) confirms that, in the QD state, the evolution of the angular fluctuations observed in simulations follows our analytical description. The symbols display the $\langle \Delta\theta^2 \rangle(t)$ fluctuations computed numerically over time, whereas the curves correspond to plots of Eq. (4), setting $c = 4$ to match their asymptotic values. Both solutions agree well for the three noise levels that we display, despite the fact that, in the course of these simulations, these systems transition from a perfect hexagonal lattice of fully aligned disks to a jammed state with random orientations. At short timescales, the angular fluctuations present a diffusive behavior with $\langle \Delta\theta^2 \rangle \simeq 2D_\theta t$, since they have

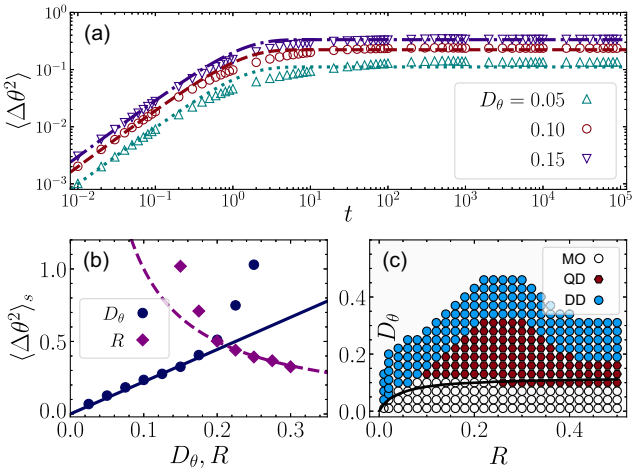

FIG. 3. (a) Mean-square fluctuations of disk orientations $\langle\Delta\theta^2\rangle$ as a function of time t, for $R = 0.3$ and three different values of D_θ. The numerical simulations (symbols) are well matched by our analytical predictions (curves) expressed in Eq. (4), especially in the asymptotic regimes. (b) Steady state of the mean-square orientation fluctuations $\langle\Delta\theta^2\rangle_s$ as a function of angular noise D_θ for fixed $R = 0.3$, and of degree of rotational eccentricity R for fixed $D_\theta = 0.15$. The numerical simulations and analytical result in Eq. (5) match very well, but only for low $\langle\Delta\theta^2\rangle_s$, as expected. (c) Phase diagram in the R-D_θ plane, where the symbols indicate the simulation results after reaching a steady state. The analytical prediction (solid black curve) for the transition from moving order to quenched disorder, given by Eq. (8), matches well the numerical results. All simulations were performed with randomly oriented initial conditions.

not yet been constrained by neighboring disks. At long timescales, they saturate at

$$\langle\Delta\theta^2\rangle_s = \frac{cD_\theta}{\beta kR}, \tag{5}$$

with characteristic crossover time $\tau \sim c/(\beta kR)$, as the retrograde forces that we will describe below drive the system to the quenched state.

Figure 3(b) compares the numerical $\langle\Delta\theta^2\rangle_s$ values after reaching the QD steady state, as a function of D_θ for fixed $R = 0.3$ (circles) and as a function of R for fixed $D_\theta = 0.15$ (diamonds), to the analytical expression in Eq. (5) vs D_θ (solid lines) and vs R (dashed lines). We find an excellent match for $\langle\Delta\theta^2\rangle_s \lesssim 0.5$ but strong deviations for higher $\langle\Delta\theta^2\rangle_s$, as expected given our small angle approximations.

Using the results above, we can determine the transition between the MO and QD phases analytically. To do this, we must first note that the repulsive forces that constrain angular fluctuations not only affect $\Delta\dot{\theta}$, but also have a component in the $-\hat{n}$ direction. Defining the mean heading of a given disk as $\hat{y} = \langle\hat{n}\rangle$, we can use Eq. (1) to compute the mean force along $\hat{y}$ as

$$\langle F_{\hat{y}}\rangle = v_0\langle\hat{n}\cdot\hat{y}\rangle + \alpha_\parallel\langle(\vec{f}\cdot\hat{n})(\hat{n}\cdot\hat{y})\rangle. \tag{6}$$

Since $\vec{f}\cdot\hat{n} \approx -(k/c)\Delta x\Delta\theta$ and $\hat{n}\cdot\hat{y} = \cos(\Delta\theta) \approx 1$ at leading order in $\Delta\theta$, we find that $\langle F_{\hat{y}}\rangle \approx v_0 - (2v_0 + \alpha_\parallel kR)\langle\Delta\theta^2\rangle_s/4$ for small angles. Using Eq. (5), we therefore obtain

$$\langle F_{\hat{y}}\rangle \approx v_0 - (2v_0 + \alpha_\parallel kR)\frac{D_\theta}{\beta kR}. \tag{7}$$

This expression shows that a larger angular noise D_θ leads to stronger retrograde forces, which will eventually surpass the self-propulsion term v_0 and produce backward motion. When this occurs, the collisions generate anti-alignment forces that result in the quenched state. Hence, the critical noise D_θ^* can be computed by imposing $\langle F_{\hat{y}}\rangle = 0$ in Eq. (7), which yields

$$D_\theta^* = \frac{v_0\beta kR}{2v_0 + \alpha_\parallel kR}. \tag{8}$$

Figure 3(c) shows that the critical noise curve $D_\theta^*(R)$ matches very well the numerical boundary between the MO and QD phases in the (R, D_θ) plane, thus validating our assumptions. The diagram also shows that QD emerges between the MO and DD phases for all $R \gtrsim 0.08$ in these simulations, and that there is an optimal $R \approx 2.26$ at which the QD state remains stable for the highest noise values. At intermediate $D_\theta \sim 0.25$, we observe a reentrant transition as a function of R, with DD for low R (where angles are not strongly confined), QD for intermediate R, and again DD for large R (where angular fluctuations disrupt the jammed QD state).

To explore how common the QD state may be, we carried out simulations beyond the limit case with only angular noise and no sideways displacements considered above, finding a QD phase for a range of anisotropic translational damping and nonzero positional noise ratios. We also searched for the QD phase in other existing models of active agents with repulsive forces that can lead to self-organization [44,55,65,66], which rely on self-alignment towards the displacement direction instead of the mechanical torques considered here. We found that QD also emerges in this type of models for a range of parameters in cases where the angular dynamics are nonlinear [55,66], but not if they are linear [44,65]. The phase diagrams resulting from these explorations are included in the Supplemental Material [58].

In conclusion, our results demonstrate and explain the emergence of a novel, noise-induced QD phase that could appear in a broad range of simulated and experimental dense active systems. Indeed, we have shown that the QD state is produced by a simple mechanical mechanism that only relies on having active components with angular noise, nonaxisymmetric rotation, and anisotropic translational damping. We emphasize that these conditions are expected to be met in many real-world systems, where self-propelled agents will typically display heading fluctuations and nonaxisymmetric

features, while presenting anisotropic damping interactions with the substrate due to their polar nature. In fact, angular noise and anisotropic damping have already been included in the description of a number of experimental active systems [33,37,56,67–69]. As a consequence, we expect the QD state to emerge in a variety of experiments (including dense, modified versions of [33,34,57]) and encourage the design of setups that could detect it.

This work was supported by the National Natural Science Foundation of China, Grant No. 62176022, and by the John Templeton Foundation, Grant No. 62213. The work of C. H. was partially funded by CHuepe Labs Inc. The work of G. L. was partially funded by China Scholarship Council.

*Corresponding author: zhan@bnu.edu.cn
†Corresponding author: cristian@northwestern.edu

[1] S. Ramaswamy, The mechanics and statistics of active matter, Annu. Rev. Condens. Matter Phys. **1**, 323 (2010).
[2] P. Romanczuk, M. B är, W. Ebeling, B. Lindner, and L. Schimansky-Geier, Active Brownian particles, Eur. Phys. J. Spec. Top. **202**, 1 (2012).
[3] J. Elgeti, R. G. Winkler, and G. Gompper, Physics of microswimmers–single particle motion and collective behavior: A review, Rep. Prog. Phys. **78**, 056601 (2015).
[4] C. Bechinger, R. Di Leonardo, H. Löwen, C. Reichhardt, G. Volpe, and G. Volpe, Active particles in complex and crowded environments, Rev. Mod. Phys. **88**, 045006 (2016).
[5] S. Ramaswamy, Active matter, J. Stat. Mech. (2017) 054002.
[6] A. Doostmohammadi, J. Ignés-Mullol, J. M. Yeomans, and F. Sagués, Active nematics, Nat. Commun. **9**, 3246 (2018).
[7] P. Guillamat, Å. Kos, J. Hardoüin, J. Ignés-Mullol, M. Ravnik, and F. Sagués, Active nematic emulsions, Sci. Adv. **4**, eaao1470 (2018).
[8] A. Martín-Gómez, D. Levis, A. Díaz-Guilera, and I. Pagonabarraga, Collective motion of active Brownian particles with polar alignment, Soft Matter **14**, 2610 (2018).
[9] C. Huepe and M. Aldana, Intermittency and clustering in a system of self-driven particles, Phys. Rev. Lett. **92**, 168701 (2004).
[10] F. Peruani, A. Deutsch, and M. Bär, Nonequilibrium clustering of self-propelled rods, Phys. Rev. E **74**, 030904(R) (2006).
[11] I. Theurkauff, C. Cottin-Bizonne, J. Palacci, C. Ybert, and L. Bocquet, Dynamic clustering in active colloidal suspensions with chemical signaling, Phys. Rev. Lett. **108**, 268303 (2012).
[12] J. Palacci, S. Sacanna, A. P. Steinberg, D. J. Pine, and P. M. Chaikin, Living crystals of light-activated colloidal surfers, Science **339**, 936 (2013).
[13] M. Paoluzzi, D. Levis, and I. Pagonabarraga, From motility-induced phase-separation to glassiness in dense active matter, Commun. Phys. **5**, 111 (2022).
[14] Y. Fily and M. C. Marchetti, Athermal phase separation of self-propelled particles with no alignment, Phys. Rev. Lett. **108**, 235702 (2012).
[15] T. Vicsek and A. Zafeiris, Collective motion, Phys. Rep. **517**, 71 (2012).
[16] T. Speck, Collective behavior of active Brownian particles: From microscopic clustering to macroscopic phase separation, Eur. Phys. J. Spec. Top. **225**, 2287 (2016).
[17] S. J. Kron and J. A. Spudich, Fluorescent actin filaments move on myosin fixed to a glass surface, Proc. Natl. Acad. Sci. U.S.A. **83**, 6272 (1986).
[18] F. J. Ndlec, T. Surrey, A. C. Maggs, and S. Leibler, Self-organization of microtubules and motors, Nature (London) **389**, 305 (1997).
[19] V. Schaller, C. Weber, C. Semmrich, E. Frey, and A. R. Bausch, Polar patterns of driven filaments, Nature (London) **467**, 73 (2010).
[20] E. F. Keller and L. A. Segel, Model for chemotaxis, J. Theor. Biol. **30**, 225 (1971).
[21] C. Dombrowski, L. Cisneros, S. Chatkaew, R. E. Goldstein, and J. O. Kessler, Self-concentration and large-scale coherence in bacterial dynamics, Phys. Rev. Lett. **93**, 098103 (2004).
[22] H. P. Zhang, A. Beer, E.-L. Florin, and H. L. Swinney, Collective motion and density fluctuations in bacterial colonies, Proc. Natl. Acad. Sci. U.S.A. **107**, 13626 (2010).
[23] J. Buhl, D. J. T. Sumpter, I. D. Couzin, J. J. Hale, E. Despland, E. R. Miller, and S. J. Simpson, From disorder to order in marching locusts, Science **312**, 1402 (2006).
[24] S. Bazazi, P. Romanczuk, S. Thomas, L. Schimansky-Geier, J. J. Hale, G. A. Miller, G. A. Sword, S. J. Simpson, and I. D. Couzin, Nutritional state and collective motion: From individuals to mass migration, Proc. R. Soc. B **279**, 3376 (2012).
[25] C. W. Reynolds, Flocks, herds and schools: A distributed behavioral model, SIGGRAPH Comput. Graph. **21**, 25 (1987).
[26] M. Nagy, Z. Ákos, D. Biro, and T. Vicsek, Hierarchical group dynamics in pigeon flocks, Nature (London) **464**, 890 (2010).
[27] B. L. Partridge, The effect of school size on the structure and dynamics of minnow schools, Anim. Behav. **28**, 68 (1980).
[28] I. D. Couzin, J. Krause, R. James, G. D. Ruxton, and N. R. Franks, Collective memory and spatial sorting in animal groups, J. Theor. Biol. **218**, 1 (2002).
[29] J. E. Herbert-Read, A. Perna, R. P. Mann, T. M. Schaerf, D. J. T. Sumpter, and A. J. W. Ward, Inferring the rules of interaction of shoaling fish, Proc. Natl. Acad. Sci. U.S.A. **108**, 18726 (2011).
[30] Y. Katz, K. Tunstrøm, C. C. Ioannou, C. Huepe, and I. D. Couzin, Inferring the structure and dynamics of interactions in schooling fish, Proc. Natl. Acad. Sci. U.S.A. **108**, 18720 (2011).
[31] A. Bricard, J.-B. Caussin, N. Desreumaux, O. Dauchot, and D. Bartolo, Emergence of macroscopic directed motion in populations of motile colloids, Nature (London) **503**, 95 (2013).
[32] A. Bricard, J.-B. Caussin, D. Das, C. Savoie, V. Chikkadi, K. Shitara, O. Chepizhko, F. Peruani, D. Saintillan, and D. Bartolo, Emergent vortices in populations of colloidal rollers, Nat. Commun. **6**, 7470 (2015).
[33] J. Deseigne, O. Dauchot, and H. Chaté, Collective motion of vibrated polar disks, Phys. Rev. Lett. **105**, 098001 (2010).
[34] J. Deseigne, S. Léonard, O. Dauchot, and H. Chaté, Vibrated polar disks: Spontaneous motion, binary collisions, and collective dynamics, Soft Matter **8**, 5629 (2012).

[35] H. Mori, Transport, collective motion, and Brownian motion, Prog. Theor. Phys. **33**, 423 (1965).

[36] A. E. Turgut, C. Huepe, H. Çelikkanat, F. Gökçe, and E. Şahin, Modeling phase transition in self-organized mobile robot flocks, in *Ant Colony Optimization and Swarm Intelligence*, edited by M. Dorigo, M. Birattari, C. Blum, M. Clerc, T. Stützle, and A. F. T. Winfield (Springer, Berlin, Heidelberg, 2008), pp. 108–119.

[37] E. Ferrante, A. E. Turgut, C. Huepe, A. Stranieri, C. Pinciroli, and M. Dorigo, Self-organized flocking with a mobile robot swarm: A novel motion control method, Adaptive Behavior **20**, 460 (2012).

[38] M. Brambilla, E. Ferrante, M. Birattari, and M. Dorigo, Swarm robotics: A review from the swarm engineering perspective, Swarm Intell. **7**, 1 (2013).

[39] S. Li, R. Batra, D. Brown, H.-D. Chang, N. Ranganathan, C. Hoberman, D. Rus, and H. Lipson, Particle robotics based on statistical mechanics of loosely coupled components, Nature (London) **567**, 361 (2019).

[40] K. H. Petersen, N. Napp, R. Stuart-Smith, D. Rus, and M. Kovac, A review of collective robotic construction, Sci. Rob. **4**, eaau8479 (2019).

[41] M. Dorigo, G. Theraulaz, and V. Trianni, Reflections on the future of swarm robotics, Sci. Rob. **5**, eabe4385 (2020).

[42] G. Oliveri, L. C. van Laake, C. Carissimo, C. Miette, and J. T. B. Overvelde, Continuous learning of emergent behavior in robotic matter, Proc. Natl. Acad. Sci. U.S.A. **118**, e2017015118 (2021).

[43] T. Vicsek, A. Czirók, E. Ben-Jacob, I. Cohen, and O. Shochet, Novel type of phase transition in a system of self-driven particles, Phys. Rev. Lett. **75**, 1226 (1995).

[44] B. Szabó, G. J. Szöllösi, B. Gönci, Z. Jurányi, D. Selmeczi, and T. Vicsek, Phase transition in the collective migration of tissue cells: Experiment and model, Phys. Rev. E **74**, 061908 (2006).

[45] E. Ferrante, A. E. Turgut, M. Dorigo, and C. Huepe, Elasticity-based mechanism for the collective motion of self-propelled particles with springlike interactions: A model system for natural and artificial swarms, Phys. Rev. Lett. **111**, 268302 (2013).

[46] G. S. Redner, M. F. Hagan, and A. Baskaran, Structure and dynamics of a phase-separating active colloidal fluid, Phys. Rev. Lett. **110**, 055701 (2013).

[47] M. E. Cates and J. Tailleur, When are active Brownian particles and run-and-tumble particles equivalent? Consequences for motility-induced phase separation, Europhys. Lett. **101**, 20010 (2013).

[48] M. E. Cates and J. Tailleur, Motility-induced phase separation, Annu. Rev. Condens. Matter Phys. **6**, 219 (2015).

[49] C. Reichhardt and C. J. O. Reichhardt, Active microrheology in active matter systems: Mobility, intermittency, and avalanches, Phys. Rev. E **91**, 032313 (2015).

[50] Y. Zhao, T. Ihle, Z. Han, C. Huepe, and P. Romanczuk, Phases and homogeneous ordered states in alignment-based self-propelled particle models, Phys. Rev. E **104**, 044605 (2021).

[51] Y. Zhao, C. Huepe, and P. Romanczuk, Contagion dynamics in self-organized systems of self-propelled agents, Sci. Rep. **12**, 2588 (2022).

[52] S. Garcia, E. Hannezo, J. Elgeti, J.-F. Joanny, P. Silberzan, and N. S. Gov, Physics of active jamming during collective cellular motion in a monolayer, Proc. Natl. Acad. Sci. U.S.A. **112**, 15314 (2015).

[53] S. Henkes, K. Kostanjevec, J. M. Collinson, R. Sknepnek, and E. Bertin, Dense active matter model of motion patterns in confluent cell monolayers, Nat. Commun. **11**, 1405 (2020).

[54] G. Lin, Z. Han, and C. Huepe, Order-disorder transition in a minimal model of active elasticity, New J. Phys. **23**, 023019 (2021).

[55] P. Baconnier, D. Shohat, C. H. López, C. Coulais, V. Démery, G. Düring, and O. Dauchot, Selective and collective actuation in active solids, Nat. Phys. **18**, 1234 (2022).

[56] H. Xu, Y. Huang, R. Zhang, and Y. Wu, Autonomous waves and global motion modes in living active solids, Nat. Phys. **19**, 46 (2023).

[57] M. Y. Ben Zion, J. Fersula, N. Bredeche, and O. Dauchot, Morphological computation and decentralized learning in a swarm of sterically interacting robots, Sci. Rob. **8**, eabo6140 (2023).

[58] See Supplemental Material at http://link.aps.org/supplemental/10.1103/PhysRevLett.131.168301 for model derivation, analytic calculations, robustness, and comparison to other models, which includes Refs. [59–63].

[59] M. Doi and S. F. Edwards, *The Theory of Polymer Dynamics* (Oxford University Press, New York, 1986), pp. 1–391.

[60] F. Peruani and I. S. Aranson, Cold active motion: How time-independent disorder affects the motion of self-propelled agents, Phys. Rev. Lett. **120**, 238101 (2018).

[61] R. Das, M. Kumar, and S. Mishra, Polar flock in the presence of random quenched rotators, Phys. Rev. E **98**, 060602 (2018).

[62] R. Das, M. Kumar, and S. Mishra, Nonquenched rotators ease flocking and memorize it, Phys. Rev. E **101**, 012607 (2020).

[63] P. Rahmani, F. Peruani, and P. Romanczuk, Topological flocking models in spatially heterogeneous environments, Commun. Phys. **4**, 206 (2021).

[64] I. Karatzas and S. E. Shreve, *Brownian Motion and Stochastic Calculus* (Springer, New York, NY, 1998), Vol. 113, pp. XXIII–470.

[65] S. Henkes, Y. Fily, and M. C. Marchetti, Active jamming: Self-propelled soft particles at high density, Phys. Rev. E **84**, 040301(R) (2011).

[66] O. Dauchot and V. Démery, Dynamics of a self-propelled particle in a harmonic trap, Phys. Rev. Lett. **122**, 068002 (2019).

[67] Y. Zheng, C. Huepe, and Z. Han, Experimental capabilities and limitations of a position-based control algorithm for swarm robotics, Adaptive Behavior **30**, 19 (2020).

[68] Z. Liu, A. E. Turgut, B. Lennox, and F. Arvin, Self-organised flocking of robotic swarm in cluttered environments, in *Towards Autonomous Robotic Systems*, edited by C. Fox, J. Gao, A. Ghalamzan Esfahani, M. Saaj, M. Hanheide, and S. Parsons (Springer International Publishing, Cham, 2021), pp. 126–135.

[69] J. Qi, L. Bai, Y. Wei, H. Zhang, and Y. Xiao, Emergence of adaptation of collective behavior based on visual perception, IEEE Internet Things J. **10**, 10368 (2023).